

Plasma-enhanced atomic layer deposition of titanium vanadium nitride

Cite as: J. Vac. Sci. Technol. A **36**, 06A103 (2018); <https://doi.org/10.1116/1.5037463>

Submitted: 24 April 2018 . Accepted: 17 August 2018 . Published Online: 10 October 2018

Mark J. Sowa, Ling Ju, Alexander C. Kozen, Nicholas C. Strandwitz, Guosong Zeng, Tomas F. Babuska, Zakaria Hsain, and Brandon A. Krick

COLLECTIONS

Paper published as part of the special topic on [2018 Special Collection on Atomic Layer Deposition \(ALD\)](#)



View Online



Export Citation



CrossMark

ARTICLES YOU MAY BE INTERESTED IN

[Status and prospects of plasma-assisted atomic layer deposition](#)

Journal of Vacuum Science & Technology A **37**, 030902 (2019); <https://doi.org/10.1116/1.5088582>

[Review Article: Stress in thin films and coatings: Current status, challenges, and prospects](#)

Journal of Vacuum Science & Technology A **36**, 020801 (2018); <https://doi.org/10.1116/1.5011790>

[Review Article: Atomic layer deposition for oxide semiconductor thin film transistors: Advances in research and development](#)

Journal of Vacuum Science & Technology A **36**, 060801 (2018); <https://doi.org/10.1116/1.5047237>



Contact Hiden Analytical for further details:
www.HidenAnalytical.com
info@hiden.co.uk


[CLICK TO VIEW](#) our product catalogue

Instruments for Advanced Science



Gas Analysis

- dynamic measurement of reaction gas streams
- catalysis and thermal analysis
- molecular beam studies
- dissolved species probes
- fermentation, environmental and ecological studies



Surface Science

- UHV TPD
- SIMS
- end point detection in ion beam etch
- elemental imaging - surface mapping



Plasma Diagnostics

- plasma source characterization
- etch and deposition process reaction kinetic studies
- analysis of neutral and radical species



Vacuum Analysis

- partial pressure measurement and control of process gases
- reactive sputter process control
- vacuum diagnostics
- vacuum coating process monitoring

Plasma-enhanced atomic layer deposition of titanium vanadium nitride

Mark J. Sowa,^{1(a)} Ling Ju,² Alexander C. Kozen,³ Nicholas C. Strandwitz,² Guosong Zeng,⁴ Tomas F. Babuska,⁴ Zakaria Hsain,⁵ and Brandon A. Krick⁴

¹Veeco—CNT, 130 Turner St, Waltham, Massachusetts 02453

²Department of Materials Science and Engineering, Lehigh University, 5 E. Packer Avenue, Bethlehem, Pennsylvania 18015

³ASEE Postdoctoral Research Fellow residing at the U.S. Naval Research Laboratory, 4555 Overlook Ave. SW, Washington DC 20375

⁴Department of Mechanical Engineering and Mechanics, Lehigh University, 19 Memorial Drive West, Bethlehem, Pennsylvania 18015

⁵Department of Mechanical Engineering and Applied Mechanics, University of Pennsylvania, 220 S 33rd St, Philadelphia, Pennsylvania 19104

(Received 24 April 2018; accepted 17 August 2018; published 10 October 2018)

The authors have studied the plasma-enhanced atomic layer deposition of $Ti_xV_{1-x}N$ using tetrakis(dimethylamido) titanium, tetrakis(dimethylamido) vanadium, and nitrogen plasma. Through modification of the ratio of TiN to VN deposition cycles, the value of x can be well controlled. X-ray photoelectron spectroscopy analyses indicate that the films are slightly nitrogen-rich with 1%–10% carbon and oxygen. Resistivity estimated from four point probe measurements were $85 \mu\Omega \text{ cm}$ (TiN) and $107 \mu\Omega \text{ cm}$ (VN) for the binary nitrides with a maximum of $182 \mu\Omega \text{ cm}$ at $x = 0.5$. The binary nitride densities were 5%–6.5% lower than bulk material literature values with interstitial stoichiometry film densities transitioning continuously from the less dense TiN (5.04 g/cm^3) to the more dense VN (5.69 g/cm^3). Crystallinity increases with vanadium content as indicated by the XRD (111) and (020) peak heights and the Scherrer crystallite size estimates. Films demonstrated excellent tribological properties with wear rates of 1.1×10^{-6} and $7.7 \times 10^{-8} \text{ mm}^3/\text{N m}$ and friction coefficients of 0.33 and 0.38 for TiN and VN, respectively. © 2018 Author(s) All article content, except where otherwise noted, is licensed under a Creative Commons Attribution (CC BY) license (<http://creativecommons.org/licenses/by/4.0/>). <https://doi.org/10.1116/1.5037463>

I. INTRODUCTION

Transition metal nitrides have long been known to have useful properties, including high melting points, extreme hardness and strength, wear resistance, corrosion resistance, high electrical conductivity, and superconductivity.¹ Furthermore, combining two transition metal nitrides to create ternary compounds has been found to produce films which have superior properties with respect to separate nitrides of the alloy.² The reported hardness, wear resistance, and corrosion protection of ternary transition metal nitrides has made them an active area of research.

TiN and VN are transition metal nitrides that share a face centered cubic structure with similar lattice parameters.³ Additionally, the two materials have been shown to be fully miscible over the entire composition range.⁴ TiVN alloys are reported in the literature produced by a variety of techniques including pulsed cathodic arc,^{5,6} sputtering,^{7–9} arc ion plating,¹⁰ mechanosynthesis,¹¹ and high temperature reactions with mesoporous carbonitride templates.¹² TiVN has been investigated for Li-battery anode.¹³ High-speed cutting tools show improved hardness and friction properties with applied TiVN coatings.¹⁴

Atomic layer deposition (ALD) is a thin film deposition technique which can produce films exhibiting excellent material quality with atomic level thickness control.^{15–17} Additional benefits include high uniformity over large area

substrates and conformality on high aspect ratio structures. These desirable characteristics are achieved by sequentially exposing the substrate to surface saturating doses of complementary chemical precursors separated by inert purge gas steps to prevent gas phase reactions. The precursor chemically reacts with surface moieties produced from the previous precursor exposure and also prepares the surface for reaction with the next precursor dose.

In addition to the thermal ALD processes discussed above, ALD processes utilizing highly reactive radicals produced by a plasma source as the coreactant have been developed.¹⁸ These widely studied plasma-enhanced ALD (PEALD) processes have several potential advantages over traditional thermal ALD, including lower temperature processing, improved film properties, more film composition options, reduced purge times, and reduced nucleation times. Due to the inadequate reactivity of potential thermal ALD nitride coreactants, such as NH_3 , PEALD is commonly investigated for growth of nitride materials.

TiN and VN have been discussed both in the thermal^{19,20} and plasma^{19,21} ALD literature but their ternary combination has yet to be reported via ALD. Few examples of ternary transitional metal nitrides exist in the PEALD literature which has so far been limited to TiNbN,²² TiHfN,²³ and TiZrN.²⁴ In this paper, we discuss the development of PEALD TiVN processes and the resulting film properties, including excellent mechanical film properties, obtained.

^{a)}Electronic mail: msowa@veeco.com

II. EXPERIMENT

The PEALD of TiVN thin films was studied. Here, the deposition conditions are discussed followed by a description of the film analysis techniques and equipment.

A. Film depositions

A Veeco—CNT Fiji system equipped with a reactor turbomolecular vacuum pump and variable conductance valve, a turbomolecular-pumped load lock, and a second generation (G2) style inductively coupled plasma source²⁵ was used to study the PEALD of TiVN.

Tetrakis(dimethylamido) titanium (TDMAT) was used for the titanium precursor and tetrakis(dimethylamido) vanadium (TDMAV) was used for the vanadium precursor. TDMAT and TDMAV were maintained at 75 and 85 °C, respectively. Process details are listed in Table I. Although, as shown below, saturated TDMAV pulsing details were established at 150 °C substrate temperature, the same pulsing conditions were utilized for this work with a 250 °C substrate. The variable conductance valve upstream from the reactor turbo was mostly closed during precursor pulsing to reduce the pumping speed and increase the residence time for improved precursor utilization. During plasma steps, the valve was fully opened to maximize the radical flux from the plasma source to the substrate. The conductance valve transitions were incorporated as part of the purges following the precursor pulse and plasma steps.

Various V:Ti ratios were obtained by mixing different ratios of the optimized VN and TiN processes. VN:TiN ratios included 0:1, 1:3, 1:2, 1:1, 2:1, 3:1, and 1:0. Total cycle count was selected to produce films that were approximately 80 nm in thickness. 80 nm is somewhat thicker than films deposited for PEALD studies but was required for the wear measurements.

Sample coupons of prime silicon (100) and silicon with 1 μm thermally grown SiO₂ were used untreated, as-received from the wafer supplier. Coupons were placed on the Fiji

substrate holder in the load lock and the load lock was evacuated to $<10^{-5}$ Torr, utilizing the load lock turbomolecular vacuum pump, for 30 min prior to transferring samples into the reactor. Thermal SiO₂ coupons were used for four point probe measurements while all other analyses utilized films deposited on the prime silicon coupons. Chamber wall temperature matched the substrate temperature. Following each deposition, the samples were moved back to the load lock and allowed to cool for 1 h at $<10^{-5}$ Torr prior to atmospheric exposure.

B. Film analyses

1. Ex situ SE

Film thickness and optical properties (633 nm), refractive index (n) and extinction coefficient (k), were measured on silicon samples with a J. A. Woollam Alpha-spectroscopic ellipsometry (SE) over a wavelength range of 380–900 nm. To gain statistical insights into the optical property uncertainties, repeat measurements were made on the Alpha-SE as well as additional measurements on a Horiba UVISEL, with a wavelength range of 225–886 nm, of the original silicon and thermal oxide samples as well as extra silicon samples included with each deposition. The SE data were evaluated with a model combining a Drude term and two Lorentz oscillators. Film resistivity can be directly calculated from the Drude term parameters²⁶ and is included in the discussion below.

2. Four point probe

Film sheet resistance values were measured using a Lucas Labs 302 Resistivity Stand with a Keithley 2400 SourceMeter. Film resistivity values reported below are the product of the four point probe sheet resistance values and the x-ray reflectivity (XRR) film thickness measurements.

3. X-ray photoelectron spectroscopy

TiVN samples were analyzed by x-ray photoelectron spectroscopy (XPS) using a Thermo K alpha XPS using monochromatic Al K α radiation (1486.7 eV). High resolution spectra of Ti2p, V2p, and N1s were obtained, and peak positions were calibrated to the adventitious carbon C1s peak = 284.8 eV. High resolution peaks were deconvoluted and fit using relative sensitivity factors obtained from the manufacturer. Reported concentration values are from the material bulk (after argon sputtering) where surface oxidation, surface adventitious carbon, and substrate components are minimized.

4. Stripe testing

Wear rate tests were performed on a custom, pin-on-disk microtribometer similar in design to a system described previously.^{27,28} Under constant loading, a ruby probe was rubbed against the film surface due to the motion of the reciprocating stage for up to 50 000 cycles. The resulting wear track was then evaluated with a profilometer to determine the wear rate.

TABLE I. Plasma-enhanced atomic layer deposition process conditions.

Step	Precursor pulse	Precursor purge	Plasma	Plasma purge
Carrier Ar (sccm)	30	100	10	30
Plasma Ar (sccm)	100	100	0	100
Plasma N ₂ (sccm)	5	5	5	5
Pump speed	Low	Low-to-high	High	High-to-low
Pressure (mTorr)	360	—	18	—
Power (W)	0	0	300	0
Time (s)	TDMAV: 0.5 TDMATi: 0.25	5	20	10
Temperature	All deposition performed at 250 °C			

5. X-ray diffraction and reflectivity

XRR measurements utilized a PANalytical Empyrean diffractometer with a Cu x-ray tube (45 mA/40 kV) at a wavelength of 1.541 Å. The configuration included a Bragg–Brentano HD mirror, soller slit, 1/8° divergence slit, and a 1/16° antiscatter slit on the incident beam path. A soller slit, parallel plate collimator, 0.1 mm receiving slit, and 0D detector were used on the diffracted beam path. All scans were performed with a 0.005° step size from 0° to 6°. The data were fit using X'Pert Reflectivity v1.3a. The XRR data were fit using a three-layer model of ALD films on Si substrate with an interfacial native SiO₂ layer (~1 nm). The density values were estimated from the critical angle of XRR data using the compositions determined by XPS.⁴³

For wide angle XRD measurements, the Bragg–Brentano HD mirror and soller slit were used. A 2θ–ω scan was utilized with a 3° offset between the incident angle ω and θ to minimize reflected x-ray intensity from the Si(100) substrate.

III. RESULTS AND DISCUSSION

A. Process development

A growth rate saturation curve for the PEALD of VN with 85 °C TDMAV and N₂ plasma at 150 °C is shown in Fig. 1. The data indicating a 0.5 s TDMAV pulse provide a saturating dose and were used for all subsequent experiments discussed in this work. Figure 1 also displays the maximum transient pressure of the different TDMAV pulse times. An in-line trap between the reactor and the pressure gauge dampens the pressure peak signature and the 0.25 s and shorter pulses do not register on the pressure gauge. Since the growth rate per cycle (GPC) stayed relatively stable while the pressure height increased substantially between 0.5 and 0.75 s, it can be concluded that the growth is saturated and is not due to depletion of the TDMAV vapor at the longer pulse time. A complete discussion of the PEALD VN process development with this chemistry will be published separately.

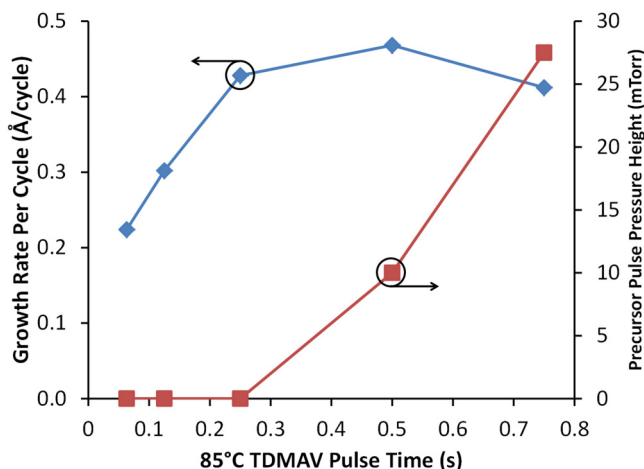


FIG. 1. 150 °C PEALD VN growth rate per cycle and precursor pulse pressure height as a function of 85 °C TDMAV pulse time.

Both TDMATi and TDMAV precursors exhibit some thermal decomposition at 250 °C leading to higher growth rates per cycle compared to saturation curves obtained at the lower temperature. At 250 °C, the GPC for the pure VN and TiN films were found to be 0.67 and 0.54 Å per cycle, respectively. The film property and process time benefits from operating in a temperature regime with a partial CVD-like thermal decomposition component outweigh any advantages to strictly maintaining pure ALD behavior at lower temperatures.

B. Composition

The composition measurement results from the XPS studies are summarized in Fig. 2. It is noted that the V and Ti levels are well controlled through the variation of the PEALD VN:TiN cycle ratio with a smooth transition between VN and TiN materials. Similar metal fraction control of ternary nitrides by PEALD cycle ratio has been previously demonstrated for TiNbN (Ref. 22) and TiHfN.²³

The TiVN were found to be slightly nitrogen-rich with the metal-to-nitrogen levels, indicated in Fig. 2 as (Ti + V)/(Ti + V + N), varying between 44% and 47%. PEALD TiNbN films were previously shown to be close to stoichiometric up to 70% Nb becoming metal-rich at higher Nb levels with 2:1 Nb:N for the Ti-free film.²² Films produced through mechanosynthesis are reported to result in films slightly substoichiometric in nitrogen.¹¹ Sputtered films have been reported as being either N-deficient²⁹ or N-rich,⁷ depending upon sputtering conditions.

Impurities were detected in the TiVN films. Carbon levels were 1%–3%. Oxygen was measured at 4%–10%, with the highest levels in the TiN and the lowest levels in the VN. The XPS data were obtained following an *in situ* sputter process which should minimize the impact of postdeposition atmospheric contaminants in the reported measurements. Carbon impurities are most likely unreacted fragments of the dimethyl amido precursor ligands. Oxygen impurities could originate from trace atmospheric sources introduced during

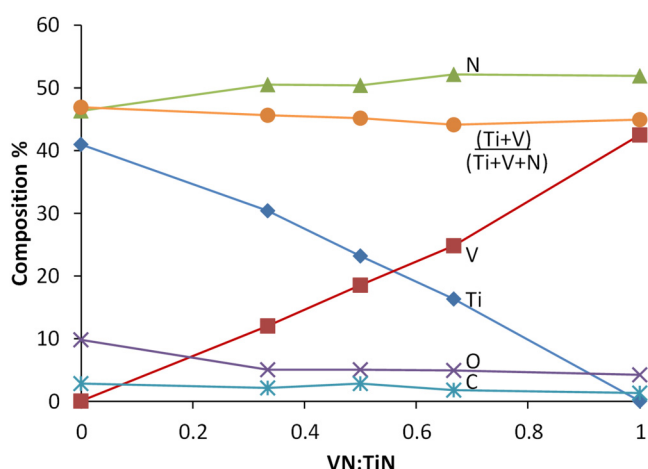


FIG. 2. XPS composition as a function of the VN:TiN cycle ratio following 60 s sputter.

sample loading or small system leaks. Oxide wall films on the multiuse reactor chamber could be a source of oxygen as could the quartz plasma tube. The relative amount of the oxygen contamination these various sources contribute is not known.

The ease with which the relatively small carbon, oxygen, and nitrogen atoms can be interstitially located or occupy vacancies in the crystal structure enables “imperfect,” non-stoichiometric films to be readily produced. The atomic scale details of the stoichiometry and impurities are not well understood and likely very important to the resulting film properties.

Subsequent analyses are presented as a function of the V:Ti stoichiometry derived from these XPS measurements rather than the VN:TiN PEALD cycle ratios.

C. Optical properties

Relatively thick films (72–104 nm from XRR) were deposited to accommodate the requirements for the wear testing. Spectroscopic ellipsometry of thicker absorbing films can lead to shifts in fitted optical property values.³⁰ The ellipsometry data were fit both solving for thickness, n , and k and solving for n and k while constraining the film thickness to the value reported by XRR. Differences between the n and k values for the fitted thickness and the fixed at the XRR value thickness varied nonsystematically up to 3.6%. Although the impact of the thick, absorbing film on the n and k calculations was considered by utilizing the XRR film thickness for fitting of the spectroscopic ellipsometry data, the reported values are still likely offset from their true values. For example, the low $n = 1.040 \pm 0.037$ for the TiN film is considerably lower than a more in-line value of $n = 1.226$ for a 40 nm TiN film grown at similar conditions on the same equipment.²²

By using multiple sets of samples and ellipsometers, we investigated the uncertainty in the n and k results. Seven sets

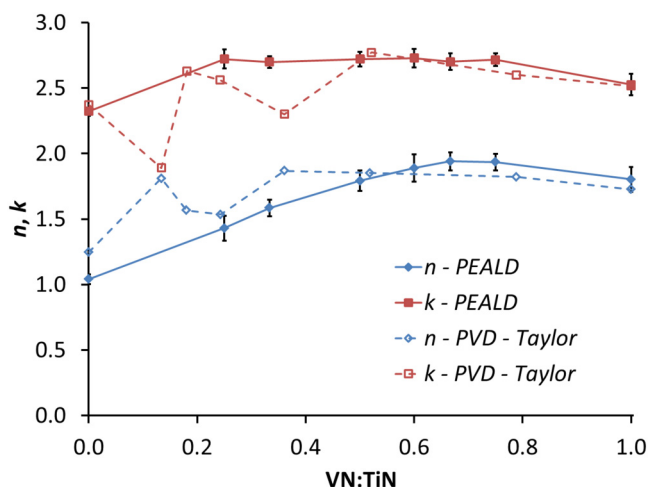


FIG. 3. Average compositional dependence of TiVN refractive index and extinction coefficient from multiple spectroscopic ellipsometry data fits. Error bars indicate \pm one standard deviation. PEALD results from this study are compared with PVD results from Ref. 31.

of n and k data were considered: (1) primary silicon samples on the Alpha-SE fitting the thickness, (2) remeasure of (1) at different sample location, (3) primary silicon samples on the Alpha-SE with thickness fixed at the XRR value, (4) primary silicon samples on the UVISSEL fitting the thickness, (5) remeasure of (4) at different sample location, (6) primary thermal oxide samples on the UVISSEL fitting the thickness, and (7) spare silicon samples on the UVISSEL fitting the thickness. The average PEALD TiVN compositional dependence along with the standard deviation error bars of n and k at 633 nm is shown in Fig. 3. The PEALD optical results are similar to literature PVD results (shown with open markers and dashed lines in Fig. 3).³¹

D. Film density

The compositional variation of the TiVN film density from the XRR measurements is shown in Fig. 4. The mass density is calculated from the electron density based on the chemical composition derived from XPS data.³² The TiN and VN PEALD nitride density values were 5%–6% lower than is reported in the literature (TiN: 5.39 g/cm³, VN: 6.0 g/cm³).¹ The lower density, compared to literature values, is likely due to the less crystalline nature of the PEALD films in this study. Reports of the TiVN density variation with composition were not found in the literature but the densities of sputtered ZrTaN,³³ TiZrN, and TiTaN (Ref. 34) were smooth and continuous between the binary nitride endpoints.

E. Crystallinity

Figure 5 shows the relevant details of XRD scans performed on the TiVN samples. The peaks near 37° and 43° correspond to the (111) and (020) reflections, respectively. As plotted in Fig. 6, both peaks are seen to shift to higher 2 θ as the film goes from titanium-rich to vanadium-rich. This is consistent with literature reports indicating the (111) TiN peak at 36.0°–36.8° while the (111) VN peak is 36.3°–38.4°. Similarly, the (020) TiN peak is reported at 41.8°–42.8° while the (020) VN peak at 42.2°–44.6°. To

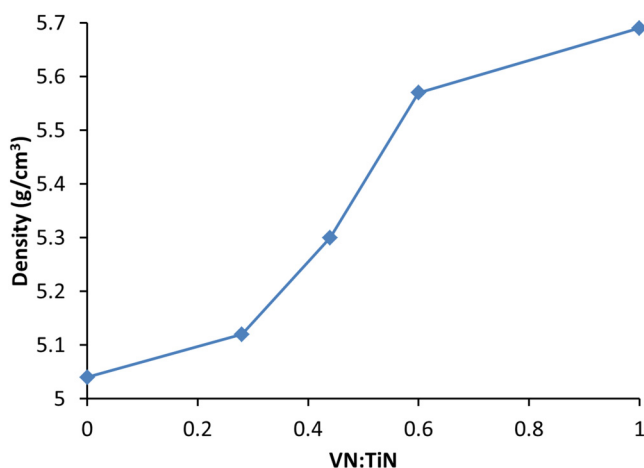


FIG. 4. PEALD TiVN density variation with stoichiometry from x-ray reflectivity measurements.

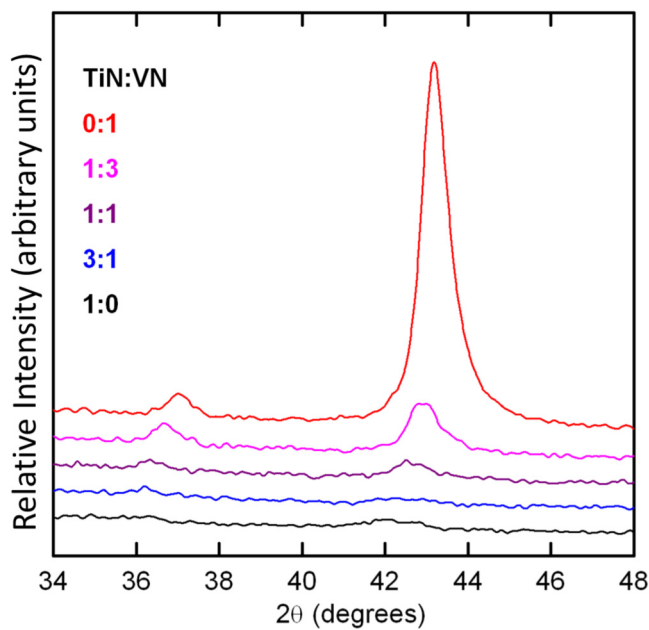


FIG. 5. Portion of XRD spectra showing the only observed peaks corresponding to (111) and (020).

obtain the position and the FWHM for the (020) peaks, the XRD data between 38° and 50° were numerically fit with a normal distribution on a linear background.

Similar XRD results are seen for most of the TiVN films from other growth methods in the literature; however, in a certain case, only one reflection was observed but that could have been due to the substrate characteristics.²⁸

The crystallite size as a function of the TiVN film stoichiometry was estimated with the Scherrer equation:

$$\tau = \frac{K\lambda}{\beta \cos \theta}. \quad (1)$$

In Eq. (1), K is a shape factor which has been set to 0.9, λ is the x-ray wavelength (0.15419 nm), β is the FWHM, and θ is

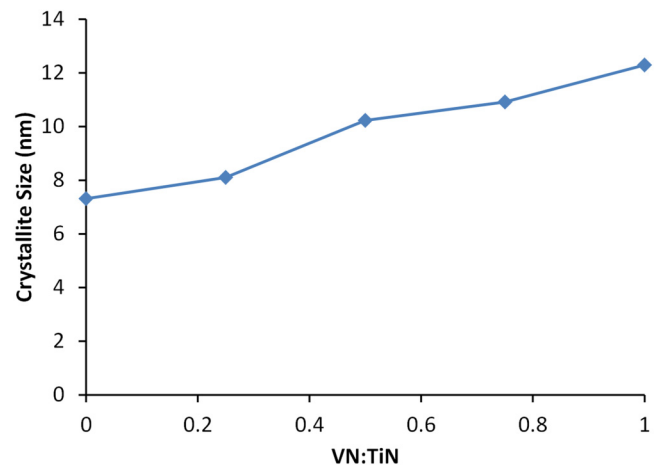


FIG. 7. Compositional dependence of the Scherrer crystallite size calculated from the XRD measurements.

the Bragg angle. Crystallite size estimates as a function of film composition are plotted in Fig. 7. Crystallite size was observed to increase from 7.3 nm for TiN to 12.3 nm for the VN. Roldán *et al.* found 5.0–5.7 nm crystallites from their mechanosynthesis derived films.¹¹ The smaller crystallite sizes found in that study could be due to the amorphization of the samples during mechanosynthesis.

F. Resistivity

The dependence of the film resistivity on V:Ti ratio is shown in Fig. 8. For comparison, the resistivity calculated from the product of the four point probe resistivity and the XRR thickness is compared with the resistivity derived from the Drude term of the spectroscopic ellipsometry model.³⁹ Pure TiN showed a lower resistivity ($85 \mu\Omega \text{ cm}$) compared to the pure VN ($107\text{--}128 \mu\Omega \text{ cm}$). Optimized thermal ALD VN exhibited a resistivity of $120 \mu\Omega \text{ cm}$.²⁰

Although the curves do not perfectly overlap, both resistivity measurements show a maximum at an intermediate stoichiometry (50% for the sheet resistance and 67% for the

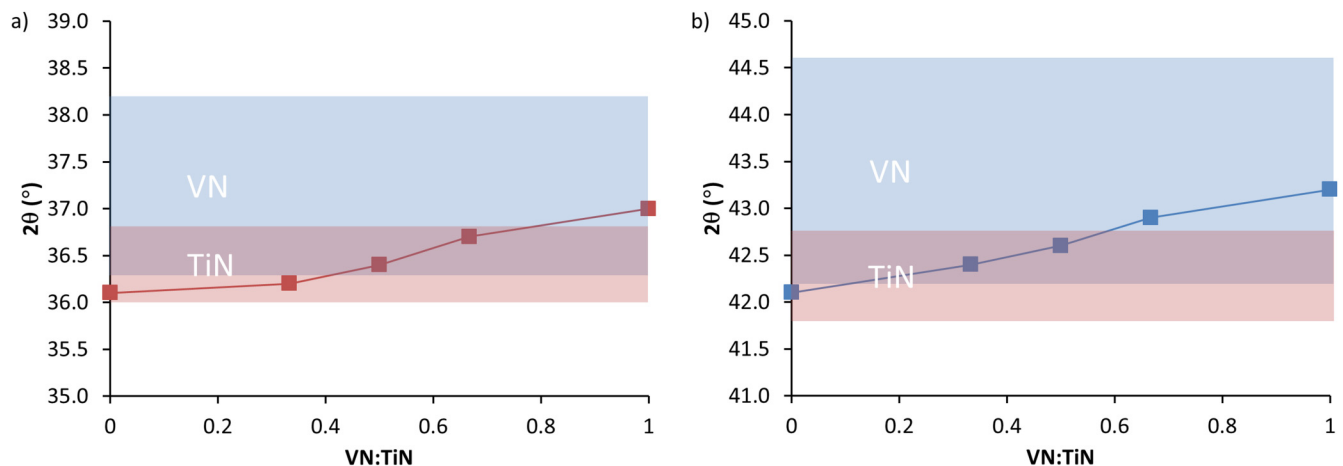


FIG. 6. XRD peak locations as a function of film stoichiometry for the (a) (111) and (b) (020) reflections. The colored bands represent the overlapping ranges of reported peak locations for the pure TiN (red/bottom) and VN (blue/top) materials.

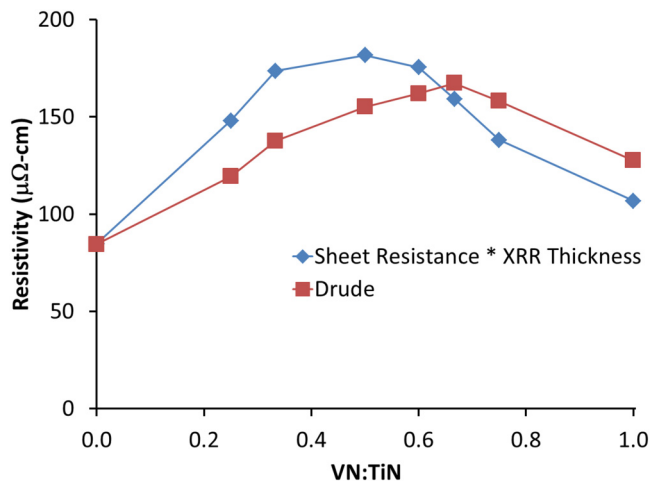


Fig. 8. Film resistivity as a function of VN:TiN ratio. The blue diamonds curve represents the resistivity derived from the four point probe sheet resistance and the XRR film thickness. The red squares curve represents the resistivity derived from the Drude term of the ellipsometric model fit.

Drude). There are not many reports of the stoichiometric resistivity variation of ternary transition metal nitrides. Abadias *et al.* report a slight resistivity maxima for cosputtered $\text{Ti}_{1-x}\text{Zr}_x\text{N}$ and a strong minima for $\text{Ti}_{1-x}\text{Ta}_x\text{N}$.³⁹ While $\text{Ti}_{1-x}\text{Ta}_x\text{N}$ film resistivity variation could be well explained from microstructure and bonding data, the $\text{Ti}_{1-x}\text{Zr}_x\text{N}$ resistivity variation with measured film properties was not obvious. Similarly, the resistivity variation in the current study does not correlate strongly with any of the measured film properties discussed above. Film stoichiometry, impurities, density, and crystallinity, reported above, are among the factors that can impact the film's measured resistivity.

The TiVN literature focuses on the mechanical properties of the ternary nitride composition, and V:Ti ratio dependence of the electrical resistivity for other production techniques was not found.

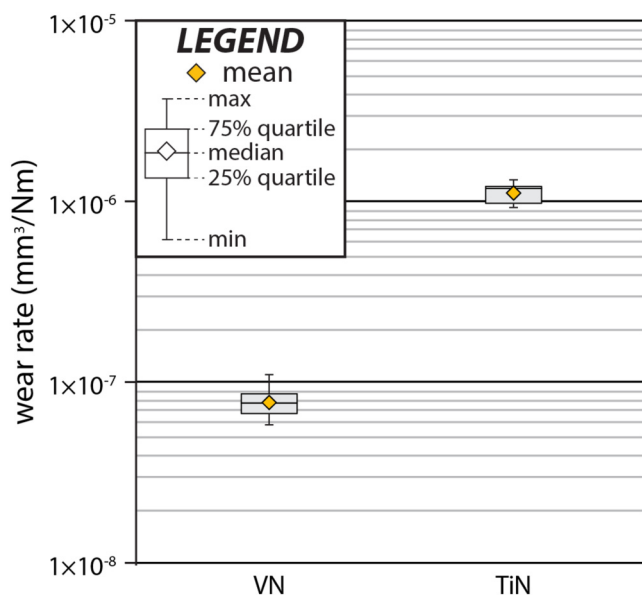


Fig. 9. Wear rates of the pure VN and TiN PEALD films.

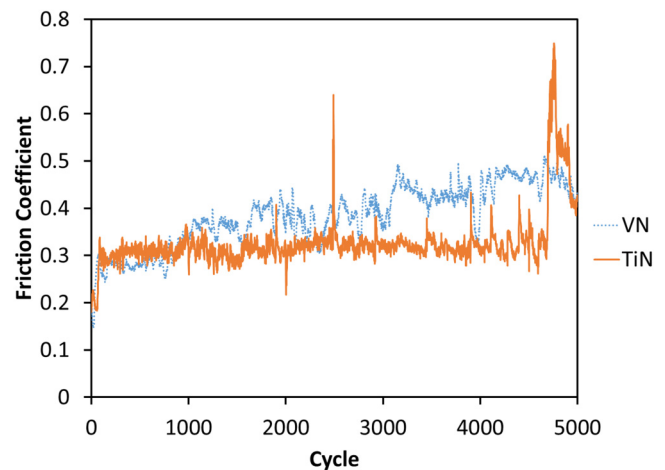


Fig. 10. Friction coefficients of the VN and TiN films as a function of the stripe testing cycle count.

VN resistivity results fit in with the 150 °C PEALD VN results of Rampelberg *et al.* falling in between the higher resistivity unannealed films ($\sim 200 \mu\Omega \text{ cm}$ for $>30 \text{ nm}$ films) and 820 °C N_2 anneal ($143 \mu\Omega \text{ cm}$) and the lower resistivity films annealed at 820 °C $\text{N}_2 + \text{H}_2$ ($93 \mu\Omega \text{ cm}$).²¹

G. TiN and VN wear rates and friction coefficients

The wear rates for the PEALD TiN and VN films are shown in Fig. 9. The PEALD TiN had a wear rate of $1.1 \times 10^{-6} \text{ mm}^3/\text{N m}$ which falls in the range of wear rates ($0.6\text{--}1.2 \times 10^{-6} \text{ mm}^3/\text{N m}$) for $1 \mu\text{m}$ 400 °C cathodic arc TiN films. VN exhibited an average wear rate of $7.7 \times 10^{-8} \text{ mm}^3/\text{N m}$, more than 14 times lower than the TiN from this study. Sputtered VN has been reported with a wear rate of $4 \times 10^{-7} \text{ mm}^3/\text{N m}$.⁴⁰ Wear rates of the intermediate stoichiometries were exceptional and will be reported separately with a more in-depth discussion of the tribological testing methodology and results.

Friction coefficients for the TiN and VN PEALD films as a function of the sliding cycle count are shown in Fig. 10. TiN had an average friction coefficient of 0.33 while the VN was slightly higher at 0.38. Cathodic arc TiN is reported to have a friction coefficient of 0.49–0.64.⁴⁰ Sputtered VN friction factor was measured at 0.28.⁴¹

Musil *et al.* found that substrate ion bombardment energy during sputter deposition of $\text{Ti}(\text{Al},\text{V})\text{N}$ films impacted the film mechanical properties.⁹ The films deposited in this study will have been subjected to ion bombardment during the plasma half cycle. Substrate ion bombardment during PEALD has been demonstrated to impact film growth rate, stoichiometry, impurities, optical properties, density, crystallinity, conductivity, residual stress, void fraction, and morphology.⁴² Although the substrate was not actively biased in the present study, ions will be accelerated across the plasma sheath (a few 10 s of volts) to the grounded electrode. The unknown (and uncontrolled) flux and energy distribution of ions to the grounded substrate surface in this study are likely impacting the film wear rates and friction coefficients

through modification of the stoichiometry, impurity levels, density, and crystallinity.

IV. CONCLUSIONS

We have demonstrated the ability to produce thin, $\text{Ti}_x\text{V}_{1-x}\text{N}_y$ films using PEALD. Through variation of the TiN:VN cycle ratio, the Ti:V ratio was predictably controlled. The metal-to-nitrogen levels varied from 44% in the TiN to 47% in the VN. Impurity levels ranged from 4% to 10% oxygen and 1% to 3% carbon.

Film resistivities were estimated from four point probe sheet resistance measurements as well as directly from the Drude term of the spectroscopic ellipsometry model. Both techniques gave qualitatively similar trends with TiN having the lowest values ($85\ \mu\Omega\text{ cm}$), VN slightly higher ($107\text{--}128\ \mu\Omega\text{ cm}$) and a maximum ($167\text{--}182\ \mu\Omega\text{ cm}$) at x values near 0.5–0.67.

XRR derived film densities were 5%–6.5% lower than literature values reported for bulk TiN and VN. Density transitioned continuously between the pure TiN and VN values.

XRD peaks corresponding to (111) and (020) peaks were observed for all films. Peak intensity trends and Scherrer crystallite size calculations suggest increasing crystallinity as deposited films became more vanadium-rich.

Excellent wear rates of 1.1×10^{-6} and $7.7 \times 10^{-8}\text{ mm}^3/\text{N m}$ were observed for the TiN and VN films, respectively. Additionally, low friction coefficients of 0.33 for the TiN and 0.38 for the VN were measured. Furthermore, the tribological properties of the ternary films exceeded the performance of the binary films to the extent that those results warrant a separate discussion.

¹L. E. Toth, *Transitional Metal Carbides and Nitrides* (Academic, New York, 1971).

²O. Knotek, W. D. Münz, and T. Leyendecker, *J. Vac. Sci. Technol. A* **5**, 2173 (1987).

³R. Sanjines, C. Wiemer, P. Hones, and F. Levy, *J. Appl. Phys.* **83**, 1396 (1998).

⁴H. Holleck, *Binäre und Ternäre Carbid- und Nitrid systeme der Übergangsmetalle* (Gebrüder Bornträger, Berlin, Stuttgart, 1984).

⁵K. E. Davies, B. K. Gan, D. R. McKenzie, M. M. M. Bilek, M. B. Taylor, D. G. McCulloch, and B. A. Latella, *J. Phys. Condens. Matter* **16**, 7947 (2004).

⁶B. A. Latella, B. K. Gan, K. E. Davies, D. R. McKenzie, and D. G. McCulloch, *Surf. Coat. Technol.* **200**, 3605 (2006).

⁷T. Deelear, S. Chaiyakun, A. Pokaipisit, and P. Limsuwan, *Mater. Sci. Appl.* **4**, 36862 (2013).

⁸M. E. Uslu, A. C. Onel, G. Ekinci, B. Toydemir, S. Durdu, M. Usta, and L. C. Arslan, *Surf. Coat. Technol.* **284**, 252 (2015).

⁹J. Musil, M. Jaroš, R. Cerstvý, and S. Haviar, *J. Vac. Sci. Technol. A* **35**, 020601 (2017).

¹⁰H. Hasegawa, A. Kimura, and T. Suzuki, *J. Vac. Sci. Technol. A* **18**, 3 (2000).

¹¹M. A. Roldán, M. D. Alcalá, and C. Real, *Ceram. Int.* **38**, 687 (2012).

¹²A. Fischer, M. Antonietti, and A. Thomas, *Adv. Mater.* **19**, 264 (2007).

¹³G. Cui, L. Gu, A. Thomas, L. Fu, P. A. van Aken, M. Antonietti, and J. Maier, *Chem. Phys. Chem.* **11**, 3219 (2010).

¹⁴N. Ichimiya, Y. Onishi, and Y. Tanaka, *Surf. Coat. Technol.* **200**, 5 (2005).

¹⁵S. George, *Chem. Rev.* **110**, 111 (2010).

¹⁶R. W. Johnson, A. Hultqvist, and S. F. Bent, *Mater. Today* **17**, 5 (2014).

¹⁷R. L. Puurunen, *J. Appl. Phys.* **97**, 121301 (2005).

¹⁸H. B. Profijt, S. E. Potts, M. C. M. van de Sanden, and W. M. M. Kessels, *J. Vac. Sci. Technol. A* **29**, 050801 (2011).

¹⁹J. Musschoot, Q. Xie, D. Deduytsche, S. Van den Berghe, R. L. Van Meirhaeghe, and C. Detavernier, *Microelectron. Eng.* **86**, 1 (2009).

²⁰M. B. Takeyama, M. Sato, H. Sudoh, H. Machida, S. Ito, E. Aoyagi, and A. Noya, *Jpn. J. Appl. Phys.* **50**, 5S1 (2011).

²¹G. Rampelberg, K. Devloo-Casier, D. Deduytsche, M. Schaeckers, N. Blasco, and C. Detavernier, *Appl. Phys. Lett.* **102**, 111910 (2013).

²²Y. T. Yemane, M. J. Sowa, J. Zhang, L. Ju, E. W. Deguns, N. C. Strandwitz, F. B. Prinz, and J. Provine, *Supercond. Sci. Technol.* **30**, 095010 (2017).

²³Yu-Shu Lin, Kuei-Wen Huang, Hsin-Chih Lin, and Miin-Jang Chen, *Solid State Commun.* **258**, 49 (2017).

²⁴Y. Kim, P. Schindler, A. L. Dadlani, S. Acharya, J. Provine, J. An, and F. B. Prinz, *Acta Mater.* **117**, 153 (2016).

²⁵M. J. Sowa, *J. Vac. Sci. Technol. A* **32**, 01A106 (2014).

²⁶P. Patsalas and S. Logothetidis, *J. Appl. Phys.* **90**, 9 (2001).

²⁷B. Krick, J. Vail, B. Persson, and W. Sawyer, *Tribol. Lett.* **45**, 185 (2012).

²⁸G. Zeng, C.-K. Tan, N. Tansu, and B. A. Krick, *Appl. Phys. Lett.* **109**, 051602 (2016).

²⁹Ö. Baran, *GUSTUJ* **7**, 2 (2017).

³⁰J. N. Hilfiker, R. A. Synowicki, and H. G. Tompkins, *Society of Vacuum Coaters, 51st Annual Technical Conference Proceedings*, Chicago, IL, 19–24 April 2008 (Society of Vacuum Coaters, Chicago, IL, 2008), p. 511.

³¹M. B. Taylor, K. E. Davies, B. K. Gan, D. R. McKenzie, M. M. M. Bilek, D. G. McCulloch, B. A. Latella, P. A. Wilksch, M. McPherson, and R. A. van den Brink, *16th National Congress of the Australian Institute of Physics Proceedings*, Canberra, ACT, 30 January–4 February 2005 (Australian Institute of Physics, Canberra, ACT, 2005), p. 268.

³²Y. Lee, B. Yoon, A. S. Cavanagh, and S. M. George, *Langmuir* **27**, 15155 (2011).

³³G. Abadias, M. B. Kanoun, S. Goumri-Said, L. Koutsokeras, S. N. Dub, and Ph. Djemia, *Phys. Rev. B* **90**, 144107 (2014).

³⁴G. Abadias, L. E. Koutsokeras, S. N. Dub, G. N. Tolmachova, A. Debelle, T. Sauvage, and P. Villechaise, *J. Vac. Sci. Technol. A* **28**, 4 (2010).

³⁵A. E. van Arkel, *Physica* **4**, 286 (1924).

³⁶A. Brager, *Acta Physicochim.* **10**, 593 (1939).

³⁷K. Becker and F. Ebert, *Zeitschrift fuer Physik* **31**, 268 (1925).

³⁸T. Onozuka, *J. Appl. Crystallogr.* **11**, 132 (1978).

³⁹G. Abadias, L. E. Koutsokeras, S. N. Dub, G. N. Tolmachova, A. Debelle, T. Sauvage, and P. Villechaise, *J. Vac. Sci. Technol. A* **28**, 541 (2010).

⁴⁰Y. Y. Guu, J. F. Lin, and C.-F. Ai, *Wear* **194**, 12 (1996).

⁴¹Y. Qiu, S. Zhang, J.-W. Lee, B. Li, Y. Wang, and D. Zhao, *Appl. Surf. Sci.* **279**, 189 (2013).

⁴²T. Faraz et al., *ACS Appl. Mater. Interfaces* **10**, 13158 (2018).

⁴³See supplementary material at <https://doi.org/10.1116/1.5037463> for fits of the XRR data.